Optical Engineering 47(5), 053603 (May 2008)

Determination of vibration parameters of a large-scale structure by measuring the visibility changes on the time-averaged images of a sinusoidal pattern fixed on it

Saifollah Rasouli, MEMBER SPIE
Institute for Advanced Studies in Basic Sciences
Zanjan 45195-1159, Iran
E-mail: rasouli@iasbs.ac.ir

Mohammad Taghi Tavassoly
University of Tehran
Physics Department
Tehran 14395-547, Iran

Abstract. Specification of vibration modes, amplitudes, and damping coefficients of structures are crucial issues in civil and mechanical engineering. Several techniques have been used for this kind of studies, including holographic interferometry, speckle interferometry, and moiré technique. But, for a large-scale structure, the modal analysis technique is usually used. We use the time-averaged digital image of a sinusoidal pattern fixed on a vibrating 6-m iron I-beam to study in-plane vibration. The study includes specification of vibrating modes, amplitudes, and damping coefficients. Using a wide-angle high-resolution digital camera, successive images of the vibrating pattern are recorded in exposure times much longer than the vibration period and much shorter than the relaxation time. The visibility measurement along the images leads to the specification of the mentioned parameters. © *2008 Society of Photo-Optical Instrumentation Engineers.* [DOI: 10.1117/1.2927460]

Subject terms: vibration analysis; time-averaged imaging; sinusoidal grating; digital image analysis; large-scale structures.

Paper 070928R received Nov. 21, 2007; revised manuscript received Feb. 20, 2008; accepted for publication Feb. 21, 2008; published online May 19, 2008. This paper is a revision of a paper presented at the SPIE Conference on Optical Measurement for Industrial Inspection IV, June 2005, Munich Germany. The paper presented there appears (unrefereed) in SPIE Proceedings Vol. 5856.

1 Introduction

The study of vibration modes, amplitudes, and damping coefficients in large-scale structures, such as bridges and buildings, is a significant topic. Several mechanical and optical techniques are available for this kind of study. Among the mechanical techniques the finite elements technique, which is called the "modal analysis" technique, is more frequently applied.[1,2] In this technique, the vibration characteristics are deduced from the responses of a structure to external activations applied at several points. In this technique, the responses are collected using accelerometers[3] or laser Doppler vibrometers[4] installed at different points of the structure. These pointwise techniques suffer from irregular mode shape estimation as a result of the lengthy data acquisition period. In addition, a large number of sensors are required for a large-scale structure.

Optical techniques, including holography, speckle, and moiré interferometry have been used for vibration studies in small-scale structures. The holography-based techniques such as classical and digital time-averaged holography, holographic interferometry, and electronic/digital speckle pattern interferometry (ESPI/DSPI) have been frequently applied for vibration studies.[5–10] While holographic techniques are very effective for measuring out-of-plane displacements of very small magnitudes, moiré methods[11–14] are well-suited for determining relatively large out-of-plane displacements. Speckle techniques have been used for recording in-plane vibrational displacement. However, as the speckles lose correlation when large displacements occur, measuring relatively large in-plane vibrational displacements is impractical. Meanwhile, the vibration study of a single curved shells by the time-averaged reflection grating principal have been suggested,[15] but it is limited to reflective curved surfaces. In this paper, we extend our previous work[16] to include the study of damping behavior and the experimental measurement of the damping coefficient. Also, the experiments are performed on a larger structure, a 6-m iron I-beam.

The main advantages of this method include the applicability to large-scale structures and to a wide range of in-plane displacements (of the order of millimeters and more), high reliability, and simplicity of application. In the presented formulation vibrations of single frequency are considered, but extension to vibrations of more than one frequency seems plausible.

2 General Description

We study the in-plane vibration component of a long beam vibrating perpendicular to its length. The study is based on processing the visibilities of the time-averaged digital images of a grating fixed on the beam. Based on some reasonable assumptions, the beam vibration is modeled by a single-frequency sinusoidal vibration and experimental results turn out to be in good agreement with the model.

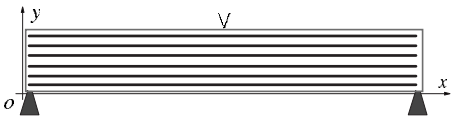

Fig. 1 Schematic side view of the beam used for formulation of the beam vibration. The beam is hit at the middle point indicated by V.

If we paste a linear periodic pattern on the surface of a large structure, such as a beam, and cause it to vibrate in the pattern plane perpendicular to the pattern lines, the image of the pattern in an imaging system, say a CCD camera, also vibrates accordingly. Then, recording the time-averaged intensity distribution on the image plane in a time interval much larger than the vibration period, in general, we observe nonuniform visibility along the pattern line direction, which resembles moiré fringes, and therefore, are sometimes called "time-averaged moiré fringes." The regions of unit normalized visibility are the nodes of the vibration mode. Twice the distance between two successive nodes divided by the magnification of the imaging system gives the wavelength of the vibrational mode. For evaluation of the amplitude, in general, one faces two different cases:

1. One is a case with nonzero visibility across the pattern, which enables amplitude evaluation by measuring the lowest visibility.
2. The other is a case where between two successive nodes there are regions of zero visibilities. Then, the distances between a node and the zero visibility regions would provide the amplitude of the vibration.

A plot of the vibration amplitude versus time is required to determine the amplitude damping coefficient.

3 Formulation

The intensity distribution on the image of a sinusoidal pattern fixed on the lateral surface of a nonvibrating beam can be represented by the following expression:

$$I(x,y)=\frac{I_0}{2}\left[1+a(x)\sin\left(\frac{2\pi}{p}y\right)\right] \quad |a(x)|\le 1, \tag{1}$$

where I_0 is the illuminating irradiance, p is the pitch of the image pattern, and $a(x)$ stands for the visibility of the pattern at distance x from the left end of the structure image. The y axis is in the pattern plane and perpendicular to the pattern strips (Fig. 1). If we put the structure into sinusoidal vibration, the image pattern vibrates sinusoidally. Assuming that the vibration along the strips is negligible, the displacement of an arbitrary point on the image pattern at time t, after the beginning of vibration, can be given by

$$L(x,t)=L_0(x)e^{-\gamma t}\sin(\omega t), \tag{2}$$

where $L_0(x)$, γ, and ω are the initial displacement amplitude of the image at distance x, the damping coefficient, and the angular frequency of the vibration, respectively. It is assumed that the displacements of points with the same x are the same. Due to vibration, the phase of the points at distance x on the image changes by

$$\Delta\phi(x,t)=\frac{2\pi}{p}L_0(x)e^{-\gamma t}\sin(\omega t) \tag{3}$$

with respect to the rest state. Thus, the intensity at point (x,y) can be given by

$$I(x,y,t)=\frac{I_0}{2}\left\{1+a(x)\sin\left[\frac{2\pi}{p}y+\Delta\phi(x,t)\right]\right\}. \tag{4}$$

Substituting $\Delta\phi(x,t)$ from Eq. (3) in Eq. (4) we get

$$I(x,y,t)=\frac{I_0}{2}\left\{1+a(x)\sin\left[\frac{2\pi}{p}y+\frac{2\pi}{p}L_0(x)e^{-\gamma t}\sin(\omega t)\right]\right\}, \tag{5}$$

or

$$I(x,y,t)=I_0\left\{1+a(x)\sin\left(\frac{2\pi}{p}y\right)\cos\left[\frac{2\pi}{p}L_0(x)e^{-\gamma t}\sin\left(\frac{2\pi}{\tau}t\right)\right]+a(x)\cos\left(\frac{2\pi}{p}y\right)\sin\left[\frac{2\pi}{p}L_0(x)e^{-\gamma t}\sin\left(\frac{2\pi}{\tau}t\right)\right]\right\}, \tag{6}$$

where ω is replaced by $2\pi/\tau$. We record the successive images of the vibrating pattern by the same exposure time T. Exposure time T is so chosen that to be considerably larger than the vibration period τ and considerably shorter than the relaxation time γ^{-1}. The time-averaged intensity at point (x,y) for m'th exposure time can be expressed as follows:

$$\bar{I}(x,y,mT)=\frac{I_0}{2}\left\{1+\frac{a(x)}{T}\int_{(m-1)T}^{mT}\sin\left(\frac{2\pi}{p}y\right)\cos\left[\frac{2\pi}{p}L_0(x)e^{-\gamma t}\sin\left(\frac{2\pi}{\tau}t\right)\right]dt+\frac{a(x)}{T}\int_{(m-1)T}^{mT}\cos\left(\frac{2\pi}{p}y\right)\sin\left[\frac{2\pi}{p}L_0(x)e^{-\gamma t}\sin\left(\frac{2\pi}{\tau}t\right)\right]dt\right\} \quad m=1,2,\ldots. \tag{7}$$

Since $\gamma^{-1}\gg T$, the changes of $e^{-\gamma t}$ in time interval T can be ignored. Now, recalling that the zero order Bessel function is[17]

$$J_0(x)=\frac{1}{2\pi}\int_0^{2\pi}\cos[x\sin(\theta)]\,d\theta, \tag{8}$$

and also

$$\frac{1}{2\pi}\int_0^{2\pi}\sin[x\sin(\theta)]\,d\theta=0, \tag{9}$$

and regarding $(2\pi/p)L_0(x)e^{-\gamma t}$ and $(2\pi/\tau)t$ as x and θ, Eq. (7) reduces to

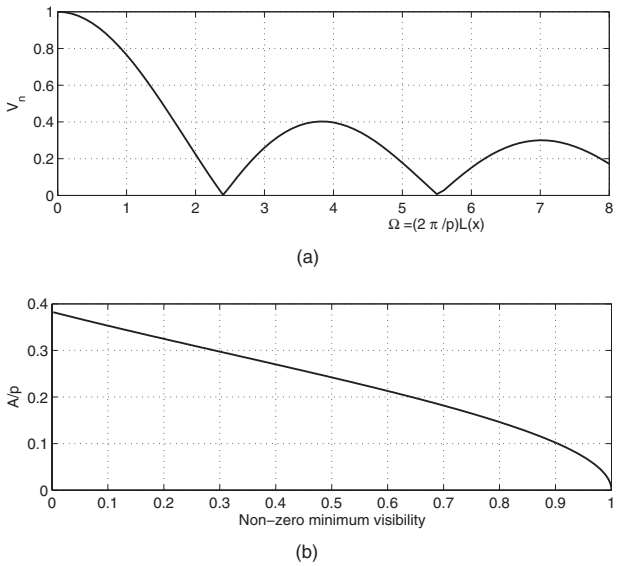

Fig. 2 Simulation of (a) the normalized visibility versus the displacement amplitude to the pitch on a sinusoidally vibrating sinusoidal pattern and (b) the ratio of the vibration amplitude A to the pattern pitch p, versus the nonzero minimum visibility on a sinusoidally vibrating sinusoidal pattern.

$$\bar{I}(x,y,mT)=\frac{I_0}{2}\left\{1+a(x)\sin\left(\frac{2\pi}{p}y\right)J_0[\Omega(x,mT)]\right\}, \qquad (10)$$

where $\Omega(x,mT)=(2\pi/p)L_0(x)\exp(-\gamma mT)$. The time interval between two successive exposures is very small compared to T. Since the vertical displacement of the pattern varies across the beam, the visibility on the time average image pattern varies with distance x. In addition, due to vibration damping, the visibility varies on successive images. On a given time-averaged image, we measure the intensity distribution along the y direction at a distance x and obtain $\bar{I}(x,:,mT)_{\max}$ and $\bar{I}(x,:,mT)_{\min}$. Thus, the visibility at a distance x from the left end of the image on the m'th image is defined by

$$V(x,mT)=\frac{\bar{I}(x,:,mT)_{\max}-\bar{I}(x,:,mT)_{\min}}{\bar{I}(x,:,mT)_{\max}+\bar{I}(x,:,mT)_{\min}} \quad m=1,2,3,\ldots. \qquad (11)$$

Substituting from Eq. (10) in Eq. (11) and dividing the result by $a(x)$, the visibility of the pattern at rest, we get the normalized visibility:

$$V_n(x,mT)=|J_0[\Omega(x,mT)]|. \qquad (12)$$

Equation (12) is plotted in Fig. 2(a). According to this plot for $V_n>0.4$ we have single value for Ω and $L(x)$. But, for $V_n<0.4$, Ω is multivalue, therefore, for specification of $L(x)$ other considerations should be considered.

3.1 *Vibration Mode Specification*

We assume that measurement takes place after formation of standing waves. Considering the boundary conditions

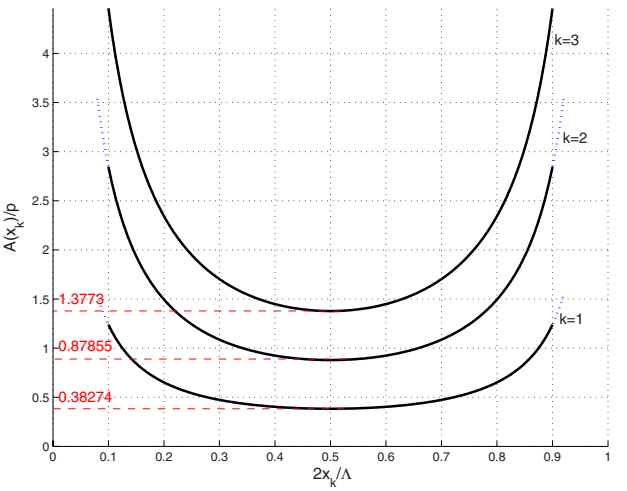

Fig. 3 Simulations of the ratio of the vibration amplitude A to the pattern pitch p, A/p, versus the distance from the zero visibility location to the nearest node location, x_k, for the first three zero visibilities for a vibration in fundamental mode.

$L(0)=0$ and $L(X)=0$, where X is the length of the beam image, the displacement of an arbitrary point on the beam image in the y direction can be given by

$$L(x,t)=A_0e^{-\gamma t}\sin\left(\frac{2\pi}{\Lambda}x\right)\sin(\omega t), \qquad (13)$$

where A_0 is the amplitude on the image of the standing wave at $t=0$, and Λ is the corresponding wavelength. The wavelength Λ_N, which corresponds to mode N, is

$$\Lambda_N=\frac{2X}{N} \quad N=1,2,3,\ldots. \qquad (14)$$

Substituting from Eqs. (13) and (14) in Eq. (12) we get

$$V_n(x,mT)=\left|J_0\left[\frac{2\pi}{p}A_0\exp(-\gamma mT)\sin\left(\frac{\pi N}{X}x\right)\right]\right|. \qquad (15)$$

The argument of Bessel function J_0 in Eq. (15) is zero at $x=(qX/N)$, $q=0,1,2,\ldots,N$. At these points, the normalized visibility is equal to 1. In fact, these points are nodal

Fig. 4 Image of one end of the used I-beam on its massive base.

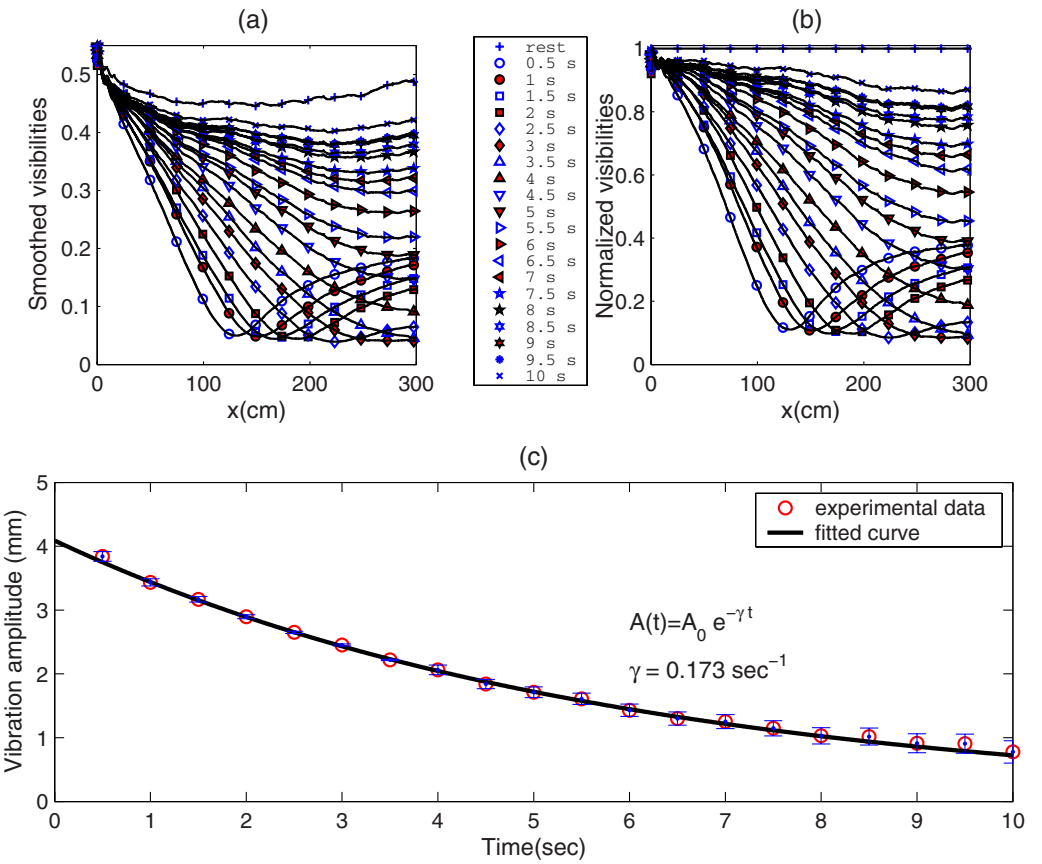

Fig. 5 Visibility curves (a) smoothed and (b) normalized across successive images of the sinusoidal pattern pasted on the vibrating I-beam. The circles in (c) are the vibration amplitudes versus time evaluated from the visibility curves in (b).

points, and their number minus one specifies the vibration mode.

3.2 *Vibration Amplitude and Damping Coefficient Specification*

For specification of the vibration amplitude two different cases are distinguished. In the first case, the minima of the visibilities are not zero. According to Eq. (15) as the argument of the Bessel function increases, the normalized visibility decreases and approaches to minimum for $x=(2s+1)(X/2N)$ $(s=0,1,\ldots,N-1)$. For example, for the first mode $N=1$, minimum visibility locates at $x=X/2$, and for the second mode $N=2$, minimum visibilities locate at $x=X/4$, $3X/4$. Thus, in this case each visibility minimum locates at halfway between two consecutive regions of $V_n=1$. Measuring the minimum visibility and substituting x by $X/2N$ in Eq. (15) one gets the amplitude from the following equation:

$$\frac{A(mT)}{p}=\frac{A_0\exp(-\gamma mT)}{p}=\frac{1}{2\pi}J_0^{-1}\{[V_n(mT)]_{\min}\}. \qquad (16)$$

Equation (16), which represents the wave amplitude to pitch ratio versus to the nonzero normalized minimum visibility, is plotted in Fig. 2(b).

In the second case, there may be one or more zero visibilities between two successive nodes $V_n=1$. These zeros are Bessel function zeros and the corresponding arguments are known quantities. Thus, from Eq. (15) we get

$$A(mT)=\frac{C_{Jk}p}{2\pi\sin[(2\pi/\Lambda)x_k(mT)]},\quad m=1,2,3,\ldots, \qquad (17)$$

where C_{Jk} is the argument for the k'th zero Bessel function, and x_k is the distance of the kth zero visibility to the nearest location of visibility 1. For example, for a vibration in the fundamental mode, the first zero visibility appears at $x_1=(\Lambda/4)(k=1, C_{J1}=2.4048)$ and Eq. (17) gives $A=0.38p$. As A/p increases, the first zero visibility splits into two zero visibilities, which move in opposite directions toward the nearest node locations, and for $A/p=0.88$, a second zero visibility appears at $x_2=\Lambda/4(k=2, C_{J2}=5.5201)$. For the further increases of A/p, other zero visibilities appear symmetrically with respect to $x=\Lambda/4$. Using Eq. (17), Fig. 3 presents plots of A/p versus the distance of the zero visibility to the location of the nearest node for $k=1,2,3$ for a vibration in the fundamental mode. In Videos 1 and 2 the vibrations of a sinusoidal pattern for different amplitudes are simulated in the first and the second vibration modes, respectively. The curves on the right side are the corresponding normalized visibility distributions. Also, vibrations of sinusoidal patterns for different amplitude to pitch ratios are simulated in the background videos, which can be

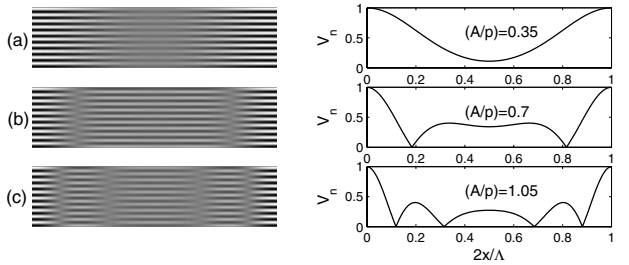

Video 1 Simulations of the time-averaged intensity distributions on a sinusoidal pattern vibrating in fundamental mode for different amplitude to pattern pitch ratios A/p: (a) 0.35, (b) 0.70, and (c) 1.05. The curves on the right show the corresponding normalized visibilities across the vibrating pattern. The video shows the successive recorded frames for different amplitude to pitch ratios (MPEG, 361 KB). [URL: http://dx.doi.org/10.1117/1.2927460.1].

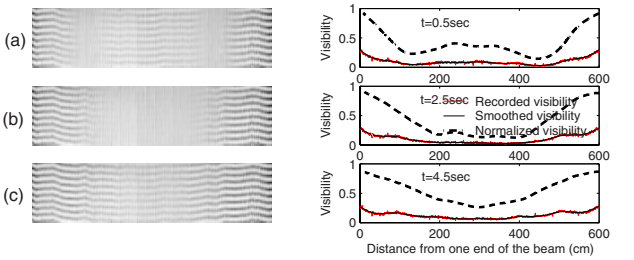

Video 3 Images of a linear sinusoidal pattern pasted on a vibrating 6.2-m-long I-beam (IPE 140) recorded witn an exposure time of 0.05 s at the times (a) 0.5, (b) 2.5, and (c) 4.5 s after the beginning of the vibration. The corresponding visibility distributions along the pattern are shown on the right. All the recorded frames and the corresponding visibilities can be observed in the background "video" (MPEG, 423 KB). [URL: http://dx.doi.org/10.1117/1.2927460.3].

watched by clicking on "video" on the corresponding captions.

To evaluate the amplitude damping coefficient the amplitudes at successive exposure times is recorded, and the sought for coefficient is derived from the plot of the amplitude versus time.

4 Experimental Works and Results

The proposed method was applied to the study of in-plane vibration of an iron I-beam, IPE 140, of length 6.2 m from Esfahan Steel Company. A sinusoidal grating programmed by a PC and printed on 30 20-$\times$7.5-cm sheets of paper. The pitch of the printed pattern was 6.2 mm. Then the sheets were pasted on one of the lateral surfaces of the beam whose ends were firmly fixed on two heavy rigid bases weighing more than 1 ton. The imaging system was Nikon D200 camera. The beam was put into vibration by hitting it at the middle with a rubber-head hammer. After each hit, the beam vibrated for a few tens of seconds and the camera recorded successive images of the vibrating pattern for data processing. The exposure time for each frame was 0.5 s and the time interval between two successive frames was 0.004 s.

Figure 4 shows an image of one end of the I-beam and the supporting base. The periodic patterns shown in Video 3 are the images of the pattern in the first, fifth, and ninth frames. The curves on the right of the patterns show their corresponding recorded, smoothed, and normalized visibilities across the images. According to these plots, the beam had been vibrating in fundamental mode. To improve the resolution of the recorded images, the symmetry of the vibrating pattern is exploited and the images of one half of the pattern were recorded and processed. For this case, the images in the first, fifth, and ninth frames, in addition to their corresponding recorded, smoothed, and normalized visibilities curves are shown in Video 4. All the recorded frames and the corresponding visibility curves can be observed in the background videos. To watch the videos click on "video" on the captions of Videos 3 and 4

Comparing the experimental visibility curves of Videos 3 and 4 with the simulation curves in Video 1, we see that the increase of the wave amplitude causes the minimum of the experimental visibility to also move toward the node, but its value does not approach zero. This is because the experimental amplitude is a slowly decaying quantity. In Figs. 5(a) and 5(b) the smoothed and normalized visibilities at successive frames are shown. Each curve represents the visibility on the image grating in a 0.5-s averaging time. As time passes, the amplitude decays and the minimum of the visibility curve moves toward the center of the beam image and then moves upward, which is in agreement with the corresponding simulations shown in Video 1. Figure 5(c) plots the amplitudes versus time obtained from the visibility curves as circles. The fitting function $A(t)=A_0e^{-\gamma t}$ on the circles led to the damping coefficient $\gamma=0.173\ \mathrm{s}^{-1}$.

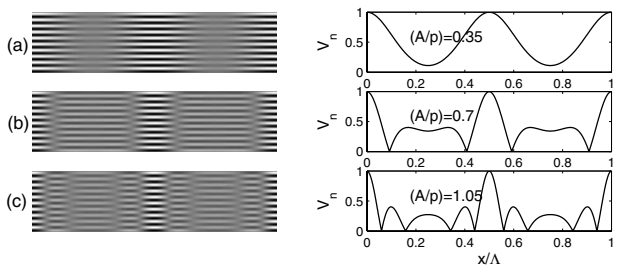

Video 2 Simulations of the time-averaged intensity distributions on a sinusoidal pattern vibrating in the second mode for different amplitude to pattern pitch ratios A/p: (a) 0.35, (b) 0.70, and (c) 1.05. The curves on the right show the corresponding normalized visibilities across the vibrating pattern. The video shows the successive recorded frames for different amplitude to pitch ratios (MPEG, 429 KB). [URL: http://dx.doi.org/10.1117/1.2927460.2].

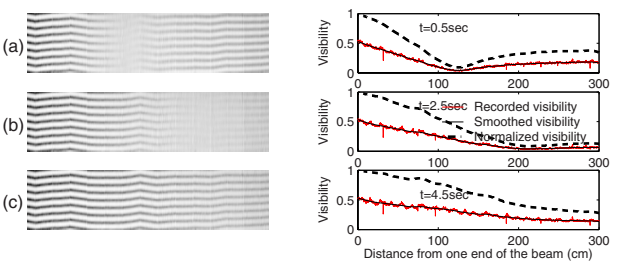

Video 4 Images of one half of the vibrating I-beam recorded at exposure times of 0.05 s at times (a) 0.5, (b) 2.5, and (c) 4.5 s after the beginning of the vibration. The corresponding visibility distributions along the pattern are shown on the right. The corresponding "video" can be observed in the background (MPEG, 457 KB). [URL: http://dx.doi.org/10.1117/1.2927460.4].

Finally, note the following concerning error estimation and measurement range. Error calculation for an 8-bits CCD of 3872×2592 pixels shows that the relative amplitude error for cases with zero visibilities is less than 0.02, but for cases with nonzero visibilities it is more than 0.04. The measurement range of the vibration amplitude from the lower side is limited by the resolution of the imaging optics, which puts a limitation on the spatial frequency of the recorded pattern and the sensitivity of CCD to intensity change. But from the upper side, practically, there is no limitation. By choosing a suitable amplitude-to-pattern pitch ratio, a desirable visibility change can be realized on the image pattern.

5 Conclusion

The presented technique is a simple, effective, and reliable method for the measurements of vibration characteristic parameters of structural beams in a wide range of vibration amplitude. It also seems that the technique can be easily applied to larger and more complex structures such as bridges, buildings, aircraft, etc. To improve the resolution for very large structures one should use several synchronized cameras.

Acknowledgments

This work was supported by Institute for Advanced Studies in Basic Sciences (IASBS).

References

1. W. T. Thomson, *Theory of Vibration with Applications*, Prentice Hall, Englewood Cliffs, NJ (1988).
2. Z. F. Fu and J. He, *Modal Analysis*, Butterworth-Heinemann, Delhi (2001).
3. Q. Qin, H. B. Li, and L. Z. Qian, "Modal identification of Tsing Ma bridge by using improved eigensystem realization algorithm," *J. Sound Vib.* **247**(2), 325–341 (2001).
4. J. Vanherzeele, S. Vanlanduit, and P. Guillaume, "Reducing measurement time for a laser Doppler vibrometer using regressive techniques," *Opt. Lasers Eng.* **45**, 49–56 (2007).
5. P. Hariharan, *Optical Holography*, Cambridge University Press, Cambridge (2000).
6. P. K. Rastogi, *Holographic Interferometry*, Springer-Verlag, Berlin (1994).
7. P. Picart, J. Leval, D. Mounier, and S. Gougeon, "Time-averaged digital holography," *Opt. Lett.* **28**(20), 1900–1902 (2003).
8. N. Demoli and I. Demoli, "Measuring surface vibrations of musical instruments using an inexpensive digital holography device, " *Opt. Eng.* **44**(9), 090502 (2005).
9. C.-C. Ma and C.-H. Huang, "Experimental whole-field interferometry for transverse vibration of plates," *J. Sound Vib.* **271**, 493–506 (2004).
10. F. M. Santoyo, M. C. Shellabear, and J. R. Tyrer, "Whole field in-plane vibration analysis using pulsed phase-stepped ESPI," *Appl. Opt.* **30**(7), 717–721 (1991).
11. O. Kafri, Y. B. Band, T. Chin, D. F. Heller, and J. C. Walling, "Real-time moire vibration analysis of diffusive objects," *Appl. Opt.* **24**(2), 717–721 (1985).
12. Y. Y. Hung, C. Y. Liang, J. D. Hovanesian, and A. J. Durelli, "Time-averaged shadow- moiré method for studying vibrations," *Appl. Opt.* **16**(6), 1717–1719 (1977).
13. K. G. Harding and J. S. Harris, "Projection moiré interferometer for vibration analysis," *Appl. Opt.* **22**(6), 856–861 (1983).
14. C. Y. Liang, Y. Y. Hung, A. J. Durelli, and J. D. Hovanesian, "Time-averaged moiré method for in-plane vibrational analysis,"*J. Sound Vib.* **62**(2), 267–275 (1979).
15. R. Ritter, U. Schulte, and C. Schulze, "Vibration of a single curved shells by the time average reflection grating principal," *Opt. Lasers Eng.* **8**, 3–15 (1988).
16. S. Rasouli and M. T. Tavassoly, "Specification of vibrational modes and amplitudes in large-scale structure by time averaging moiré technique," *Proc. SPIE* **5856**, 746–755 (2005).
17. G. Arfken, *Mathematical Methods for Physicists*, Academic Press Inc., Orlando, Florida (1985).

Saifollah Rasouli received his BSc degree from Shahid Beheshti University, Iran, in 1994 and his MSc and PhD degrees from Institute for Advanced Studies in Basic Sciences (IASBS), Iran, in 1997 and 2007, respectively. He is currently a postdoctoral researcher in the Physics Department of the IASBS. His research interests are the application of moiré techniques in the studies of structural vibrations, atmospheric turbulence, and nonlinear optics. From 1997 to 2003, he was a research assistant in the optics lab at the IASBS. His interests also include moiré technique, interferometry, optical metrology, fringe analysis, fiber index profile measurements, holography, and photosensitive materials.

Mohammad Taghi Tavassoly is a professor of physics in the Physics Department of the University of Tehran. His research interests include interferometry, Fresnel diffraction from phase objects, light scattering from rough surfaces, optical metrology, and moiré technique applications. He has been collaborating with the Institute for Advanced Studies in Basic Sciences (IASBS) in Zanjan since 1992.